CERN-PH-TH/2011-025, KCL-PH-TH/2011-03, SU–ITP–11/04,
UMN–TH–2936/11, FTPI–MINN–11/03, SLAC-PUB-14372

Neutrino Fluxes from NUHM LSP Annihilations in the Sun

John Ellis,[1,*] Keith A. Olive,[2,†] Christopher Savage,[3,‡] and Vassilis C. Spanos[4,§]

[1] *TH Division, Physics Department, CERN, 1211 Geneva 23, Switzerland;*
Theoretical Physics and Cosmology Group, Department of Physics,
King's College London, London WC2R 2LS, UK
[2] *William I. Fine Theoretical Physics Institute, School of Physics and Astronomy,*
University of Minnesota, Minneapolis, MN 55455, USA;
Department of Physics and SLAC, Stanford University, Palo Alto, CA 94305, USA
[3] *The Oskar Klein Centre for Cosmoparticle Physics,*
Department of Physics, Stockholm University,
AlbaNova, SE-10691 Stockholm, Sweden
[4] *Institute of Nuclear Physics, NCSR "Demokritos", GR-15310 Athens, Greece*

(Dated: April 27, 2011)

We extend our previous studies of the neutrino fluxes expected from neutralino LSP annihilations inside the Sun to include variants of the minimal supersymmetric extension of the Standard Model (MSSM) with squark, slepton and gaugino masses constrained to be universal at the GUT scale, but allowing one or two non-universal supersymmetry-breaking parameters contributing to the Higgs masses (NUHM1,2). As in the constrained MSSM (CMSSM) with universal Higgs masses, there are large regions of the NUHM parameter space where the LSP density inside the Sun is not in equilibrium, so that the annihilation rate may be far below the capture rate, and there are also large regions where the capture rate is not dominated by spin-dependent LSP-proton scattering. The spectra possible in the NUHM are qualitatively similar to those in the CMSSM. We calculate neutrino-induced muon fluxes above a threshold energy of 10 GeV, appropriate for the IceCube/DeepCore detector, for points where the NUHM yields the correct cosmological relic density for representative choices of the NUHM parameters. We find that the IceCube/DeepCore detector can probe regions of the NUHM parameter space in addition to analogues of the focus-point strip and the tip of the coannihilation strip familiar from the CMSSM. These include regions with enhanced Higgsino-gaugino mixing in the LSP composition, that occurs where neutralino mass eigenstates cross over. On the other hand, rapid-annihilation funnel regions in general yield neutrino fluxes that are unobservably small.

*Electronic address: John.Ellis@cern.ch
†Electronic address: olive@physics.umn.edu
‡Electronic address: savage@fysik.su.se
§Electronic address: spanos@inp.demokritos.gr

I. INTRODUCTION

One of the most actively pursued strategies for detecting supersymmetric dark matter particles (LSPs) is the search for signatures of the annihilations of LSPs inside the Sun or Earth[1, 2]. The principle for detection is to search for the passage through a large detector in ice or water of muons produced by the interactions of energetic neutrinos released in the LSP dark matter annihilation process. There have been extensive studies of this potential experimental signature in many variants of the MSSM, and experiments such as IceCube/DeepCore [3–6] are starting to chip away at the MSSM parameter space.

We recently re-analyzed [7] this potential signature in the framework of the MSSM with all the supersymmetry-breaking spin-1/2 and -0 mass parameters $(m_{1/2}, m_0)$ constrained to be universal at the GUT scale (the CMSSM) [8], imposing the requirement that the LSP should provide the density of dark matter inferred from WMAP [9] and other experiments. In the CMSSM, where the supersymmetry breaking trilinear mass parameters, A_0 are also taken to be universal at the GUT scale, the resulting relic density is found to lie in the WMAP range only along relatively narrow strips in the $(m_{1/2}, m_0)$ plane for fixed $\tan\beta$ and A_0 [10, 11]. These correspond to the coannihilation strip, where the mass of the lightest neutralino is close to the mass of the lightest charged slepton (usually the mostly right-handed stau); the heavy Higgs funnel, found at large $\tan\beta$ and large $(m_{1/2}, m_0)$, where the neutralino mass is close to half the heavy Higgs mass and rapid annihilations of neutralinos are mediated by the s-channel exchange of heavy Higgs scalars and pseudoscalars; and the focus-point region which is typically found at very large values of m_0 when the μ parameter (an output of the minimization of the Higgs potential in the CMSSM) is driven to small values and the neutralino picks up a more significant Higgsino component.

In our previous work [7], we found that the LSP capture rate was not in general dominated by scattering on protons inside the Sun via spin-dependent couplings, but that an important role was often played by spin-independent scattering on heavier nuclides. We also found that, in many regions of the CMSSM parameter space, LSP capture and annihilation would not be in equilibrium, and that the annihilation rate would be correspondingly reduced. We also analyzed the uncertainties in the magnitude of the potential muon-neutrino signal due to uncertainties in the composition of the Sun and in the scattering matrix elements. We found that the CMSSM might be detectable in IceCube/DeepCore along (some part of) the WMAP strip in the focus-point region of the $(m_{1/2}, m_0)$ plane, and near the low-$m_{1/2}$ tip of the WMAP strip in the coannihilation region [7, 12].

In this paper we extend these previous studies to models with one or two degrees of non-universality in the soft supersymmetry-breaking contributions to the Higgs doublets, the NUHM1 [13, 14] and NUHM2 [14–16]. One of our primary objectives is to understand the circumstances under which such relatively high neutrino fluxes may be attained in these models and, conversely, whether the relatively low rates usually found in the CMSSM are specific to that model. More generally, we seek to lay a basis for systematic comparisons of the physics capabilities of different detection strategies in (relatively) simple variants of the MSSM.

Supersymmetric dark matter searches [6, 17, 18] are complementary to searches for supersymmetry at accelerators [19, 20]. At the moment, the latter are sensitive primarily to the spin-1/2 and -0 mass parameters $m_{1/2}$ and m_0, and are less sensitive to the non-universality parameters that appear in the NUHM1,2. For example, global likelihood fits [21] currently yield similar 68 and 95% confidence-level preferred regions in the $(m_{1/2}, m_0)$ planes of the

CMSSM and NUHM1. It is therefore particularly interesting to know whether direct and indirect dark matter searches offer ways to differentiate between these models.

The NUHM1,2 offer additional mechanisms to bring the relic LSP density into the WMAP range, in addition to the coannihilation, rapid-annihilation and focus-point possibilities mentioned above in the context of the CMSSM. For example, there are distinctive regions of NUHM parameter space where Higgsino-gaugino mixing in the LSP is enhanced by level-crossing in the neutralino mass matrix, bringing the relic density into the WMAP range. Alternatively, the LSPs may annihilate rapidly through direct-channel heavy Higgs H, A poles even if $m_{1/2}, m_0$ and $\tan\beta$ are relatively small. It was shown in [21] that the collider prospects for sparticle detection are rather different in the NUHM1 low-mass rapid-annihilation region than they are in the CMSSM, whereas the favoured rates for direct LSP detection via scattering on nuclei were broadly similar in the CMSSM and the NUHM1 (though the uncertainties were greater in the latter case). Therefore, it is interesting to study the prospects in this region for LSP detection via the energetic neutrinos produced by annihilation inside the Sun.

The layout of this paper is as follows. In Section II we recall briefly some general features of the NUHM1,2 and discuss other inputs into the rate calculations. Then, in Section III we explore the solar annihilation rates in some generic slices through the NUHM1 parameter space, finding that they are enhanced in regions with relatively large Higgsino components in the LSP as may occur for specific relations between μ and $m_{1/2}$ where there is level crossing. In Section IV we extend our analysis to slices through the NUHM2 parameter space. Section V summarizes our conclusions.

We find that whereas the neutrino flux may be observable in regions with enhanced Higgsino-gaugino mixing, analogously to the enhancement along the focus-point WMAP strip in the CMSSM, the flux is generically unobservably low in the rapid-annihilation funnels. This suggests that the observation of a high-energy solar neutrino flux in the IceCube/DeepCore experiment is a potential diagnostic for large mixing and level crossing in the neutralino mass matrix, and specifically of the relation between μ and $m_{1/2}$, which is a potential tool for identifying non-universal Higgs mass parameters.

II. PREAMBLE

A. The NUHM1 and NUHM2 Parameter Spaces

In the CMSSM, the free parameters are the supposedly universal supersymmetry-breaking parameters $m_{1/2}, m_0$ and A_0, as well as $\tan\beta$. The Higgs mixing superpotential parameter μ and the bilinear supersymmetry-breaking parameter B_0, and hence the pseudoscalar Higgs mass m_A, are then determined using the electroweak vacuum conditions, with a sign ambiguity in μ. The sign of the discrepancy between the experimental value of $g_\mu - 2$ and the value calculated within the Standard Model suggests that $\mu > 0$, and CMSSM analyses are often presented in $(m_{1/2}, m_0)$ planes for $\mu > 0$ and fixed values of $\tan\beta$ and A_0. Although much of our NUHM analysis is for $\mu > 0$, we also consider the possibility of a negative sign. The value of A_0 is notoriously unconstrained, see, *e.g.*, [22], and for definiteness we set it to zero in what follows.

In the NUHM1, the soft supersymmetry-breaking contributions to the masses of the two MSSM Higgs doublets, m_1 and m_2, are assumed to be equal, but are allowed to differ from m_0. The extra degree of freedom may be used to treat either m_A or $|\mu|$ as a free parameter.

On the other hand, in the NUHM2, the two soft supersymmetry-breaking contributions to the masses of the MSSM Higgs doublets are allowed to vary independently, and the two extra degrees of freedom may be used to treat both m_A and $|\mu|$ as free parameters. Analyses of the NUHM1 and NUHM2 parameter spaces are often presented in planes spanned by pairs of the quantities $m_{1/2}, m_0, m_A$ and μ for some fixed values of $\tan\beta$ and the other parameters, and we present some examples below which are selected from the analysis in [14]. Since a frequentist likelihood analysis favours relatively small values of $m_{1/2}$ and m_0 in both the CMSSM and NUHM1 [21], we concentrate here on NUHM1 and NUHM2 planes with relatively low values of either $m_{1/2}$ and m_0. We note, however, that a complete likelihood analysis of the NUHM2 is yet to be performed.

B. Spin-Dependent and -Independent Scattering Rates

When calculating the LSP annihilation rates inside the Sun, the key particle physics inputs—apart from the choice of supersymmetric model—are the matrix elements for dark matter scattering on the nuclides inside the Sun. It is often assumed that LSP capture in the Sun is dominated by spin-dependent scattering on hydrogen but, as discussed in [7], spin-independent scattering on heavier nuclei actually dominates in generic regions of the CMSSM parameter space. Figure 1 displays contours of the ratio of the solar dark matter annihilation rate calculated using only spin-dependent scattering to the total annihilation rate including also spin-independent scattering in (left) the CMSSM $(m_{1/2}, m_0)$ plane for $\tan\beta = 10$, $A_0 = 0$ and $\mu > 0$, and (right) the NUHM1 $(m_{1/2}, m_0)$ plane for $\tan\beta = 10$, $A_0 = 0$ and $\mu = 500$ GeV. Regions excluded because there is no consistent electroweak symmetry breaking (EWSB) have dark pink shading, those with a charged LSP have brown shading, and those in conflict with $b \to s\gamma$ [23] measurements have green shading. Regions to the left of the black dashed (red dash-dotted) line are inconsistent with the absence at LEP of charginos (a Higgs boson) [24–26]. We recall that there is a theoretical uncertainty ~ 1.5 GeV in the calculation of m_h in the CMSSM, which induces an uncertainty ~ 50 GeV in values of $m_{1/2}$ along the red dash-dotted line. The recent LHC direct exclusion regions in the CMSSM $(m_{1/2}, m_0)$ plane [19, 20] are somewhat weaker than the indirect LEP Higgs constraint shown here. The pale pink band is favoured by the BNL measurement of $g_\mu - 2$ [27–29], at the $\pm 1(2) - \sigma$ level along the dashed (solid) lines, but we do not impose this as a constraint on our analysis. In the CMSSM case (left panel), we see that spin-dependent scattering is dominant only at small $m_{1/2}$ and large m_0. In the NUHM1 case (right panel), we see that spin-dependent scattering is subdominant at small $m_{1/2}$, becoming more important along the WMAP-compatible strip with $m_{1/2} \sim 1000$ GeV. However, spin-independent scattering is important even here, and in the following analysis all calculations of the annihilation rates include the contributions from both spin-dependent and -independent scattering.

The uncertainties in the spin-independent scattering matrix element include those in the ratios of the light quark masses, the octet contribution, σ_0, to the pion-nucleon σ term, $\Sigma_{\pi N}$, and the value of $\Sigma_{\pi N}$ itself [30–34]. The largest uncertainty is due to $\Sigma_{\pi N}$, for which we used the value 64 MeV as our default in [7], whilst also exploring the implications of other values. The second-largest uncertainty is due to that in σ_0, for which we used the value 36 MeV as our default. We assume the same default values in this analysis. As discussed in more detail in Refs. [7, 33], different measurements for $\Sigma_{\pi N}$ and σ_0 lead to variations in the spin-independent scattering cross-section by a factor of $\sim$2–3 and the choice of experimental values for these two parameters significantly impacts the spin-independent scattering contribution to capture

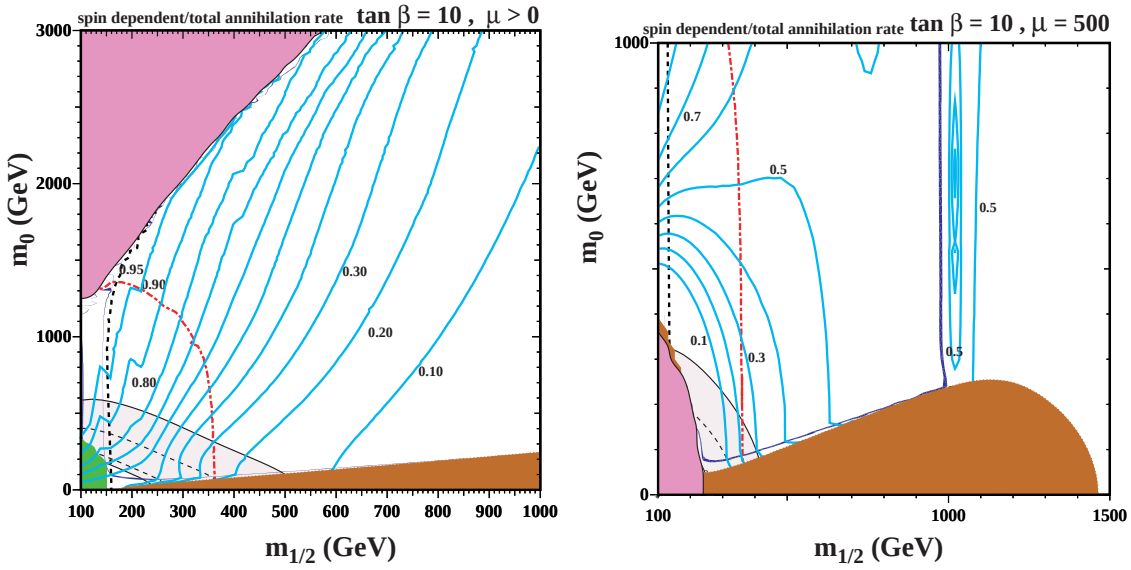

FIG. 1: *Sample* $(m_{1/2}, m_0)$ *planes for* $\tan\beta = 10$ *and* $A_0 = 0$ *in (left) the CMSSM for* $\mu > 0$ *and (right) the NUHM1 for* $\mu = 500$ *GeV, showing regions excluded because there is no consistent electroweak vacuum (dark pink shading), or because there is charged dark matter (brown shading), or because of a conflict with* $b \to s\gamma$ *measurements (green shading). Only regions to the right of the black dashed (red dash-dotted) line are consistent with the absence at LEP of charginos (a Higgs boson). The turquoise strips are favoured by the determination of the cold dark matter density by WMAP and other experiments [9], and the light pink band is favoured by the BNL measurement of* $g_\mu - 2$. *We also show contours of the ratio of the solar dark matter annihilation rate calculated using only spin-dependent scattering to the total annihilation rate including also spin-independent scattering.*

in the Sun. If $\Sigma_{\pi N}$ were smaller, the total annihilation rate would decrease, and the ratio of the solar dark matter annihilation rate calculated using only spin-dependent scattering to the total annihilation rate including also spin-independent scattering shown in Figure 1 would increase. By comparison, the uncertainties in the light quark mass ratios are much less significant.

The principal uncertainty in the spin-dependent matrix element is the contribution of strange quarks to the nucleon spin, Δ_s, with the uncertainties due to g_A and the SU(3)-octet nucleon matrix elements being significantly smaller. The range $-0.06 \geq \Delta_s \geq -0.12$ was considered in [7], and was found to induce an uncertainty in the annihilation rate that was $\sim 10\%$, considerably smaller than the others considered. In the following we take the central value $\Delta_s = -0.09$ [35], which was adopted in [7] as the default value.

C. Capture/Annihilation Rates and Neutrino/Muon Fluxes

We compared in [7] the rates estimated in various alternative solar models. We found that there was at most a 4% difference in the annihilation rates between the two models of Serenelli *et al.* [36] (AGSS09 and AGSS09ph) based upon recent abundance estimates [37], and assumed the AGSS09 model as our default. We do the same here, performing a

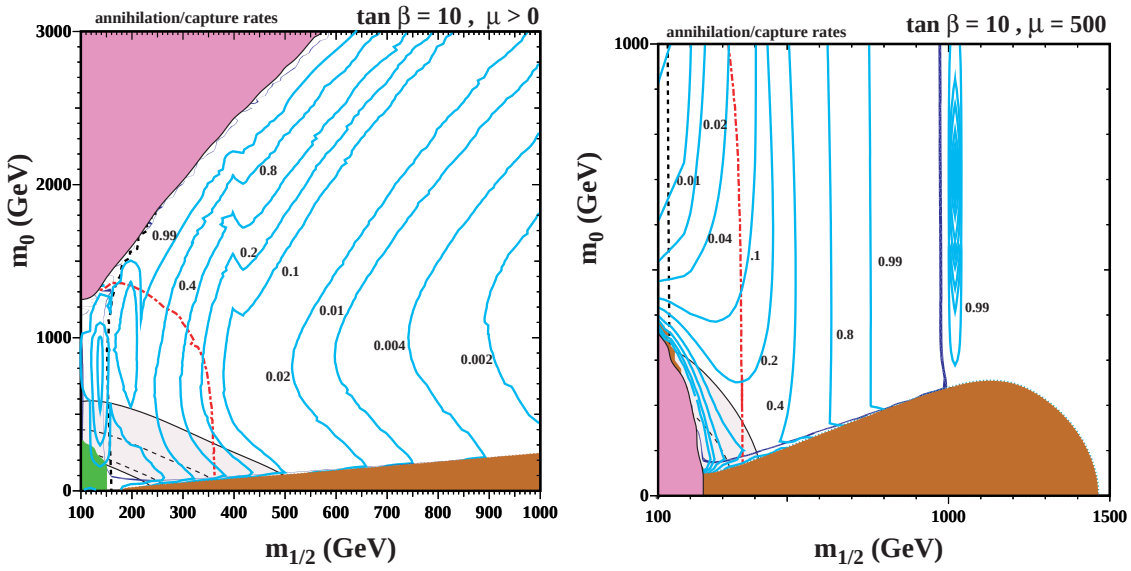

FIG. 2: *The same CMSSM plane (left) and NUHM1 plane (right), displaying also contours of the ratio of solar dark matter annihilation and capture rates. Equilibrium corresponds to a ratio of unity, which is approached for small* $m_{1/2}$ *and large* m_0 *in the CMSSM, and near a vertical strip with* $m_{1/2} \sim 1000$ *GeV in the NUHM1 example.*

full numerical integration over the radial profile of the Sun when determining the capture rates [1].

In modelling the dark matter halo, we assume a non-rotating isothermal sphere with an rms speed of 270 km/s, a disk rotation speed of 220 km/s, and a local dark matter density of 0.3 GeV/cm^3. If the calculated neutralino relic density is below the WMAP observed relic density, we assume that only a fraction of the local dark matter density, equal to the ratio of the neutralino and WMAP dark matter relic densities, is attributable to neutralinos. As in [7], we do not address other halo models in this paper, but note that our results would scale linearly with the local dark matter density as equilibrium between capture and annihilation is approached.

However, as discussed extensively in [7], equilibrium is not in general reached in the CMSSM, and an example is shown in the left panel of Figure 2, namely the $(m_{1/2}, m_0)$ plane for $\tan\beta = 10, A_0 = 0$ and $\mu > 0$. The dark blue contours are for different ratios of the annihilation and capture rates, and we see that equilibrium is reached only for small $m_{1/2}$ and large m_0. The right panel of Figure 2 shows the corresponding contours in the NUHM1 $(m_{1/2}, m_0)$ plane for $\tan\beta = 10, A_0 = 0$ and $\mu = 500$ GeV, where we see that equilibrium is approached only near a vertical strip with $m_{1/2} \sim 1000$ GeV. In the following we calculate annihilation rates without relying on the assumption of equilibrium.

The neutralino annihilations produce high-energy neutrinos which, through interactions with matter, will induce muons in or around a detector such as IceCube/DeepCore [3–6]. The IceCube detector has outfitted $\sim$1 km^3 of ice at the South Pole with optical sensors

[1] Using the simpler Gould approximation [38] would have yielded rates differing from the exact results by at most 6%, as was shown in [7].

to observe the Cerenkov light produced by the passage of muons through the ice. The large volume allows for sensitivity to very low neutrino fluxes. However, the relatively large spacing between sensors severely limits the sensitivity to lower energy muons (below 100 GeV) which are the largest portion of the neutrino-induced muon spectra arising from annihilations in the Sun. To improve the sensitivity to these important lower-energy muons, a portion of the IceCube volume, referred to as DeepCore, has been outfitted with more densely packed sensors.

The ability of IceCube/DeepCore to detect the flux from a given supersymmetric model depends on various factors such as the muon spectra, the neutrino backgrounds, and the method by which IceCube/DeepCore will analyze their results. However, to a very rough approximation, IceCube can detect muon fluxes on the order of 10 or 10^2 /km^2/yr above $\sim$100 GeV and DeepCore can detect muon fluxes on the order of 10^2 or 10^3 /km^2/yr above $\sim$10 GeV. In this paper, we primarily examine the latter case: total fluxes above 10 GeV. DeepCore can detect muons down $\sim$10 GeV; however, the analysis threshold may turn out to be somewhat higher: Ref. [39] suggests an analysis threshold of $\sim$35 GeV is reasonable, while Ref. [40] suggests 25–30 GeV is more likely (but possibly as low as 20 GeV) [2]. In addition, the efficiency of detecting muons (or, equivalently, the effective area of the detector) falls with decreasing muon energy. Our results are not significantly affected by our choice of a 10 GeV threshold as we use only an order-of-magnitude estimate of the IceCube/DeepCore sensitivity to the total muon flux above this energy. Our results are only affected if the flux is predominantly just above threshold (*e.g.* between 10 and 25 GeV), which is only expected to be the case for very light neutralinos ($m_\chi \ll 100$ GeV or $m_{1/2} \ll 200$ GeV) [3].

We use the results of the WimpSim simulation [41] (as used within DarkSUSY [42]) to calculate the spectra of the neutrinos produced by the annihilations and the corresponding spectra of neutrino-induced muons in IceCube/DeepCore. More details of the neutralino capture/annihilation processes and the determination of the neutrino/muon fluxes may be found in Ref. [7].

III. REPRESENTATIVE STUDIES IN THE NUHM1

A. Comparison with the CMSSM in the $(m_{1/2}, m_0)$ Plane

The left panel of Figure 3 displays the neutrino-induced muon fluxes calculated in the $(m_{1/2}, m_0)$ plane for the typical CMSSM scenario with $\tan\beta = 10, A_0 = 0$ and $\mu > 0$ introduced above. We recall that this plane has two narrow strips where the LSP density falls within the range allowed by WMAP and other measurements [9], which are coloured turquoise. One is the coannihilation strip close to the boundary of the forbidden charged-

[2] Triggering of two of IceCube/DeepCore's optical modules—which is possible for muons with energies as low as $\sim$10 GeV—is sufficient to detect a muon. However, two-module events suffer from extremely poor angular resolution. Muons that trigger three optical modules (which requires somewhat higher muon energies) yield much better track reconstruction and allow the analysis to be restricted to muons consistent with neutrinos coming from the direction of the Sun.

[3] The 10 GeV threshold was chosen and the bulk of the work done in this paper was performed prior to the availability of threshold estimates from Refs. [39, 40]. As this choice does not significantly affect our results, we have chosen to keep the current threshold in our analysis.

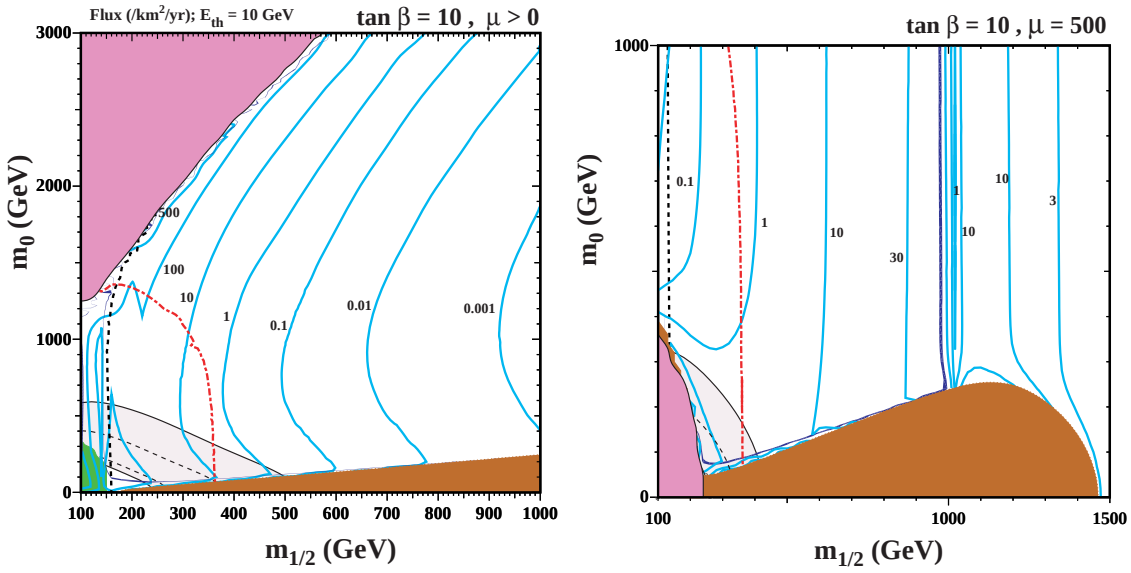

FIG. 3: *The $(m_{1/2}, m_0)$ planes for $\tan\beta = 10$ and $A_0 = 0$ in (left) the CMSSM and (right) the NUHM1 for $\mu = 500$ GeV. The solid (light blue) lines are contours of the neutrino-induced muon fluxes above 10 GeV in units of events/km^2/yr. The shadings and other contours have the same meanings as in Figure 2.*

LSP region at low m_0, and the other is the focus-point strip close to the EWSB boundary at large m_0.

As was discussed extensively in [7] and shown in the left panel of Figs. 1 & 2, at large $m_{1/2}$ it is usually not appropriate to assume that the LSP capture cross-section is dominated by spin-dependent interactions, nor that there is equilibrium between capture and annihilation. Accordingly, as already mentioned, neither assumption is made in this and subsequent plots. The solid (blue) lines are contours of the neutrino-induced muon fluxes above 10 GeV in units of events/km^2/yr. As seen in the left panel of Figure 3, the neutrino rate is potentially detectable in IceCube/DeepCore along a significant stretch of the focus-point strip, but apparently undetectable along the portion of the coannihilation strip that is compatible with the LEP Higgs constraint. As discussed in [7], the neutrino fluxes in the CMSSM are generally larger for $\tan\beta = 55$ along the coannihilation strip (though still not observable in IceCube/DeepCore), and smaller along the focus-point strip than they are for the $\tan\beta = 10$ case shown. We also recall that when $\tan\beta = 55$, there is also a third region compatible with the dark matter density constraint, namely a rapid-annihilation funnel at large $m_{1/2}$, where the rate is far too small to be detectable by IceCube/DeepCore.

The right panel of Figure 3 displays the neutrino-induced muon fluxes to be expected in a sample $(m_{1/2}, m_0)$ plane in the NUHM1, again with $\tan\beta = 10$ and $A_0 = 0$, but now with fixed $\mu = 500$ GeV. In this case, an excluded charged LSP region again appears at small m_0 though with a different shape from the CMSSM, and the EWSB boundary has moved to small $m_{1/2}$ and m_0. Here it is m_A^2 that is driven negative rather than μ^2 as in the CMSSM. There is a region favoured by $g_\mu - 2$ that is almost excluded by the LEP Higgs constraint, and there is a coannihilation strip, as in the CMSSM, that follows the EWSB boundary. There is also a near-vertical extension of the coannihilation strip at $m_{1/2} \sim 1000$ GeV, that appears thanks to the freedom in the NUHM1 of independently adjusting the μ parameter.

It occurs along a line where a particular relation between μ and $m_{1/2}$ induces level crossing in the neutralino mass matrix as $m_{1/2}$ is increased relative to μ, and thereby leads to increased Higgsino-gaugino mixing that brings the LSP density down into the WMAP range. To the right of this strip, the relic density falls below the WMAP range. This strip is the only part of this particular NUHM1 plane where the neutrino-induced muon flux approaches detectability in IceCube/DeepCore, rising above 30 /km^2/yr, thanks to the enhanced Higgsino-gaugino mixing.

One of the key questions in our analysis will be the extent to which the freedom in the NUHM1,2 to vary μ and/or m_A provides this and other opportunities for IceCube/DeepCore detection of neutrinos that are absent in the CMSSM.

B. NUHM1 $(\mu, m_{1/2})$ Planes

We now illustrate further the behaviour of this IceCube/DeepCore-friendly WMAP strip with enhanced Higgsino-gaugino mixing, first in some representative $(\mu, m_{1/2})$ planes. Figure 4 displays planes for $\tan\beta = 10$ with (upper left) $m_0 = 300$ GeV and (upper right) $m_0 = 500$ GeV: both values of m_0 are in the range favoured by a frequentist analysis of the NUHM1 parameter space [21]. In each case we see EWSB boundaries at large $|\mu|$ and small $m_{1/2}$ where $m_A^2 < 0$, and regions with $\mu < 0$ that are disfavoured by $b \to s\gamma$. In the upper left panel, we also see charged LSP regions at large $|\mu|$ and $m_{1/2}$. In each case, there is a pair of diagonal WMAP-compatible strips visible at $|\mu| \sim m_{1/2}/2$ where the Higgsino-gaugino mixing is enhanced, which are only weakly dependent on m_0 and are compatible with the LEP Higgs constraint for large enough $m_{1/2}$. The neutrino-induced muon flux above 10 GeV is potentially detectable along essentially all of these diagonal WMAP-compatible strips in both panels, though decreasing as $|\mu|$ and $m_{1/2}$ increase. These strips constitute extensions of the IceCube/DeepCore-friendly strip seen in the right panel of Figure 3, which has $\mu = 500$ GeV and $m_{1/2} \sim 1000$ GeV, to different values of these NUHM1 parameters. The red dot-dashed curve is the contour for $m_h = 114$ GeV and one should preferably lie above this curve, though one should recall that there is a 1.5 GeV uncertainty in the theoretical calculation of m_h. Nevertheless, fluxes above the Higgs limit still reach above 500 /km^2/yr. For $m_0 = 300$ GeV, the $g-2$ constraint would prefer lower values of $m_{1/2}$ in potential conflict with the Higgs bound – though the muon fluxes are quite large where both constraints are satisfied. At $m_0 = 500$ GeV, the $g-2$ is not satisfied within 2σ anywhere on the plot. We note that there is another WMAP strip slightly above the region with no EWSB. This strip corresponds to the heavy Higgs funnel where $2m_\chi \approx m_A$ and would not be present in the CMSSM at $\tan\beta = 10$. However, neutrino-induced muon fluxes are too small along these strips to be observed in IceCube/DeepCore.

Similar diagonal strips with enhanced Higgsino-gaugino mixing are seen in the lower left panel of Figure 4 for $\tan\beta = 20$ and $m_0 = 500$ GeV, though the muon fluxes are generally smaller. However, the diagonal strip for $\mu > 0$ has a part where $g_\mu - 2$ lies within the favoured range and the muon flux is > 300 /km^2/yr. As in the previous panels of Figure 4, the WMAP-compatible strips corresponding to the funnel and close to the EWSB boundary have muon fluxes which are unobservably low. In the lower right panel of Figure 4 for $\tan\beta = 55$ and $m_0 = 500$ GeV we see that, whilst the EWSB boundary is located similarly to the previous panels, the charged LSP region has advanced considerably, as has the region excluded by $b \to s\gamma$. At this value of $\tan\beta$, $\mu < 0$ is not consistent with RGE running. We also note that the diagonal strip with enhanced Higgsino-gaugino mixing has merged

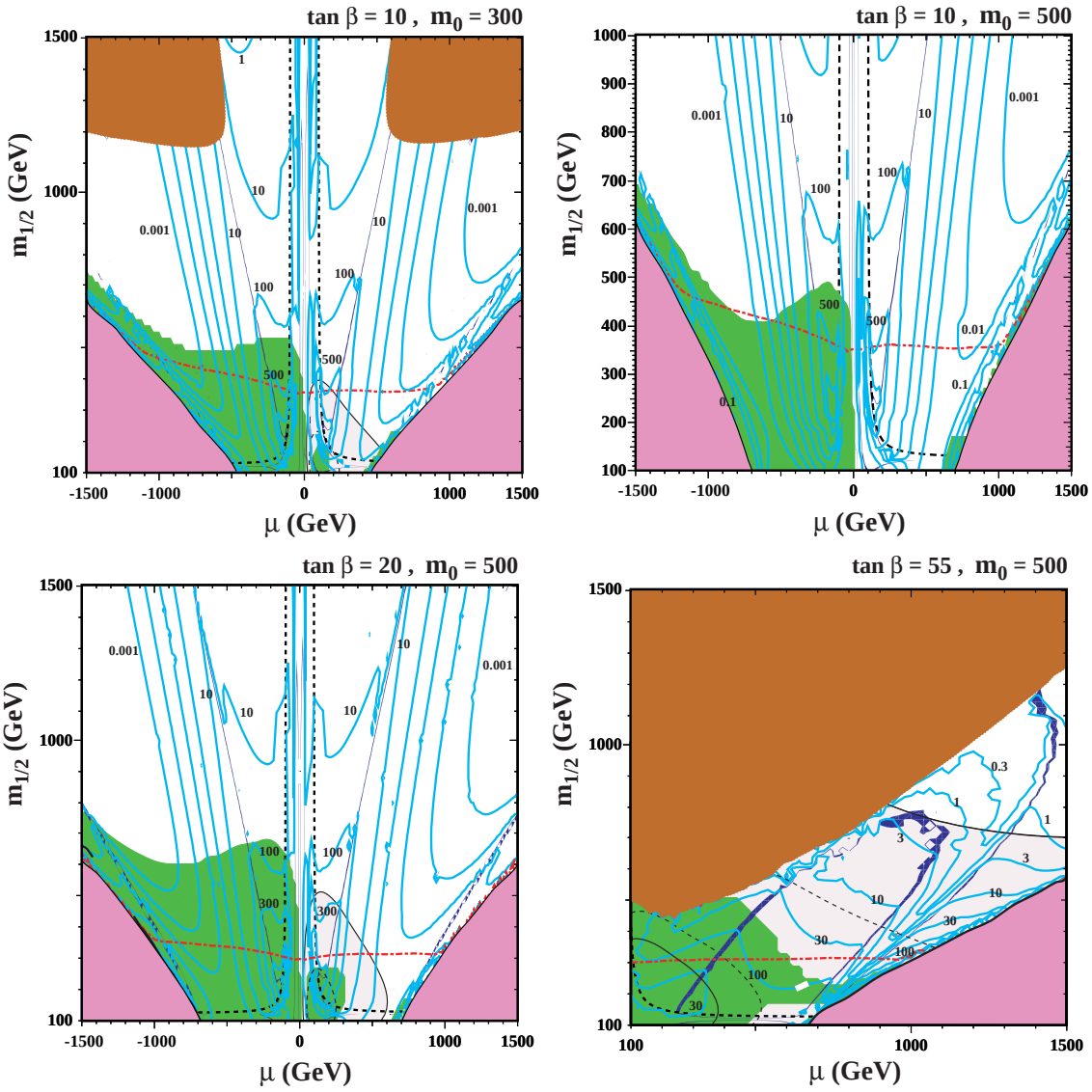

FIG. 4: *The* $(\mu, m_{1/2})$ *planes in the NUHM1 for* $A_0 = 0$ *and (upper)* $\tan\beta = 10$*, (left)* $m_0 = 300$ *GeV and (right)* $m_0 = 500$ *GeV, (lower)* $m_0 = 500$ *GeV and (left)* $\tan\beta = 20$ *and (right)* $\tan\beta = 55$*. The shadings and contours have the same meanings as in Figure 3.*

with the rapid-annihilation funnel, with both sides of the funnel now easily discernible. The muon fluxes where $b \to s\gamma$ is acceptable are $\lesssim 50$ /km^2/yr and large enough to be detectable by IceCube/DeepCore in the lower part of the transition strip, for values of $m_{1/2}$ above the bounds imposed by the LEP Higgs constraints and well with the 1σ bounds from $g-2$ (denoted by the dashed black curves). The entire region with $m_{1/2}$ below 700-800 GeV yields values of $g_\mu - 2$ in the range favoured by experiment. In contrast to the cases with lower $\tan\beta$, the funnel region now also has neutrino fluxes that are sufficiently large to be observable [4].

[4] We note that equilibrium is established along the transition strip in all cases, but not along the funnel except at very large $\tan\beta$. We also note that spin-dependent scattering is dominant at low $|\mu|$ for

C. NUHM1 (μ, m_0) Planes

In order to explore further the IceCube/DeepCore-friendly region, in Figure 5 we display NUHM1 planes for $\tan\beta = 10$ with (upper left) $m_{1/2} = 300$ GeV and (upper right) $m_{1/2} = 500$ GeV (again, both values of $m_{1/2}$ are in the range favoured by a frequentist analysis of the NUHM1 parameter space [21]), and for $m_{1/2} = 500$ GeV with (lower left) $\tan\beta = 20$ and (lower right) $\tan\beta = 55$. We see in both the upper panels EWSB boundaries at large $|\mu|$ and small m_0, charged LSP regions at smaller $|\mu|$ and m_0, and regions excluded by $b \to s\gamma$ when $\mu < 0$. When $m_{1/2} = 500$ GeV, there is a small region (shaded black) between the stau LSP region and the EWSB boundary where the LSP is a right-handed selectron (or smuon). As in the right panel of Figure 3, we see in both of the upper panels WMAP-compatible strips at roughly fixed values of $|\mu|$ related to the values of $m_{1/2}$, along which the muon flux above 10 GeV is potentially detectable: above 500 events/km^2/yr for (upper left) $m_{1/2} = 300$ GeV and $\mu \sim 200$ GeV, and above 100 events/km^2/yr for (upper right) $m_{1/2} = 500$ GeV and $\mu \sim 300$ GeV. As already commented, along these strips the fluxes are enhanced by Higgsino-gaugino mixing. We note that only part of the strip for $m_{1/2} = 300$ GeV is compatible with the LEP Higgs constraint, whereas all the $m_{1/2} = 500$ GeV strip is compatible. There are no parts of the IceCube/DeepCore-friendly strips in regions favoured by $g_\mu - 2$. In both panels, there are WMAP-compatible extensions of these strips to larger μ at $m_0 \sim 100$ GeV, due to coannihilation, which segue into funnel strips close to the EWSB boundary. However, these do not yield neutrino fluxes interesting for IceCube/DeepCore. In both upper panels, equilibrium is established and spin-dependent scattering is dominant along the transition strip, whilst the opposite is true along the funnel.

Turning now to the lower panels in Figure 5, we see that as $\tan\beta$ increases with fixed $m_{1/2} = 500$ GeV the EWSB boundary moves away to larger $|\mu|$, the charged LSP region rises to larger m_0 and (for $\tan\beta = 55$) the $b \to s\gamma$ exclusion extends to $\mu > 0$ as well as the visible parts of the half-plane with $\mu < 0$. In the lower left panel for $m_{1/2} = 500$ GeV and $\tan\beta = 20$ we see near-vertical WMAP-compatible strips with $|\mu| \sim 300$ GeV where Higgsino-gaugino mixing is enhanced and the neutrino flux is favourable for IceCube/DeepCore, and part of the strip for $\mu > 0$ is also favoured by $g_\mu - 2$. This interesting region then bends into a near-horizontal coannihilation strip, resembling those in the upper panels, where the neutrino-induced muon flux is mostly unfavourable. As $|\mu|$ increases at low m_0, the LSP changes from a mostly right-handed stau to a right-handed $\tilde{e}/\tilde{\mu}$. The muon flux is also small in the funnel that follows the stau LSP boundary. Turning finally to the lower right panel in Figure 5, we clearly see a two-sided diagonal funnel where the rapid annihilation via direct-channel heavy Higgs poles brings the relic density into the WMAP-compatible range, albeit with a relatively low muon flux. We also see that the strip with enhanced Higgsino-gaugino mixing is less vertical and with a lower flux than previously, though still IceCube/DeepCore-friendly. In this case, the $g - 2$ constraint is satisfied over much of the plane.

$\tan\beta = 10$ and 20, but subdominant at larger $|\mu|$ for all values of $\tan\beta$.

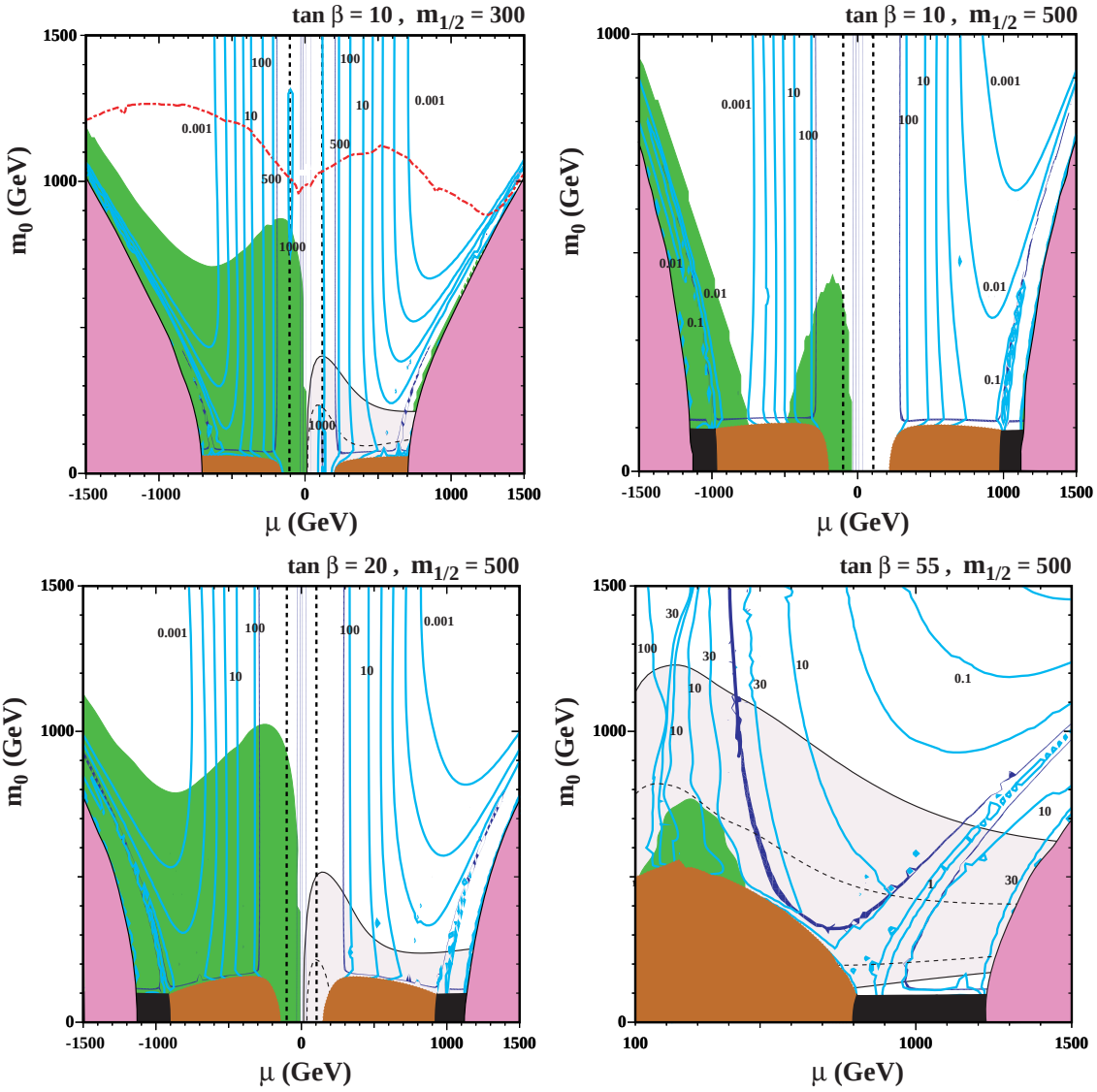

FIG. 5: *The* (μ, m_0) *planes in the NUHM1 for* $A_0 = 0$ *and (upper)* $\tan\beta = 10$*, (left)* $m_{1/2} = 300$ *GeV and (right)* $m_{1/2} = 500$ *GeV, (lower)* $m_{1/2} = 500$ *GeV and (left)* $\tan\beta = 20$ *and (right)* $\tan\beta = 55$*. In the black regions the LSP is the right-handed selectron or smuon, and the other shadings and contours have the same meanings as in Figure 3.*

D. NUHM1 $(m_A, m_{1/2})$ Planes

Figure 6 displays some representative $(m_A, m_{1/2})$ planes in the NUHM1 for $A_0 = 0$ and $\tan\beta = 10$ with (upper left) $m_0 = 300$ GeV and (upper right) $m_0 = 500$ GeV. In both cases, we see that the EWSB requirement excludes a triangular region at large m_A and small $m_{1/2}$ where μ^2 is driven negative, whereas $b \to s\gamma$ excludes a band at small m_A. There is a region favoured by $g_\mu - 2$ in the left plane that is again almost excluded by the LEP Higgs constraint. In each case, a WMAP-compatible strip runs parallel to the EWSB boundary, extending to small m_A at $m_{1/2} \sim 125$ GeV. There is also a diagonal funnel where LSPs annihilate rapidly though direct-channel Higgs poles, because $m_\chi \sim m_A/2$, and there are WMAP strips on

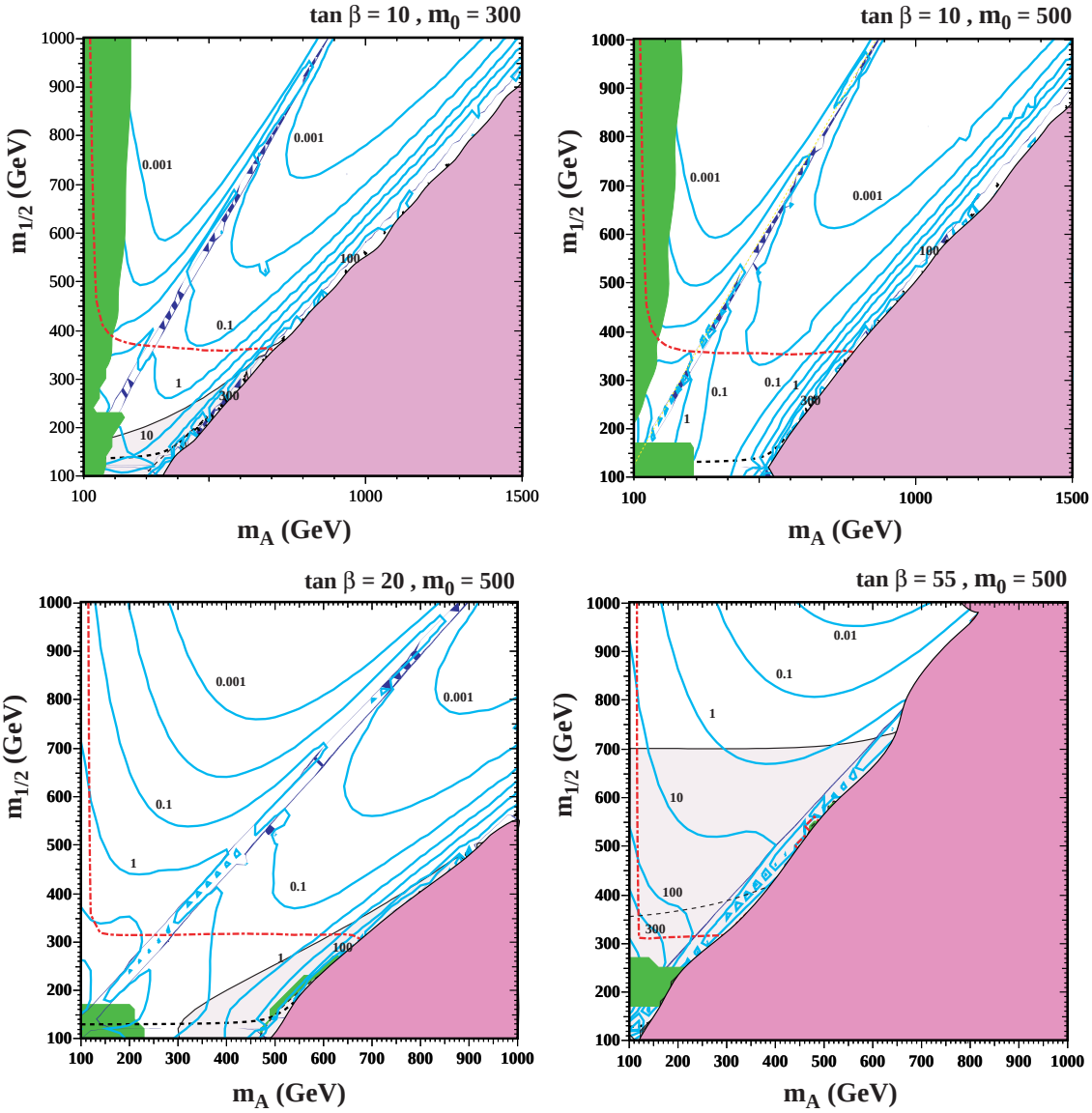

FIG. 6: *The* $(m_A, m_{1/2})$ *planes in the NUHM1 for* $A_0 = 0$ *and (upper row)* $\tan\beta = 10$ *and (left)* $m_0 = 300$ *GeV, (right)* $m_0 = 500$ *GeV, (lower row) for* $m_0 = 500$ *GeV and (left)* $\tan\beta = 20$ *and (right)* $\tan\beta = 55$*. The shadings and contours have the same meanings as in Figure 3.*

either side of this funnel. The neutrino flux is very unfavourable along the funnel, since the neutrino-induced muon flux above 10 GeV is $\ll 10$ events/km^2/yr. However, a signal may be observable in IceCube/DeepCore along the EWSB boundary, where the muon flux above 10 GeV lies in the range 10 to 100 events/km^2/yr. As we have seen before, equilibrium is established and spin-dependent scattering is dominant along the transition strip near the EWSB boundary, in contrast to the funnel regions where equilibrium is not established and spin-independent scattering is dominant.

Turning now to the lower row of plots in Figure 6 for (left) $\tan\beta = 20$ and (right) $\tan\beta = 55$, both with $m_0 = 500$ GeV, we see that the EWSB boundary is broadly similar, whereas the region forbidden by $b \to s\gamma$ is much reduced. The WMAP-compatible rapid-

annihilation funnel is clearly visible for $\tan\beta = 20$, but folds into the EWSB boundary strip for $\tan\beta = 55$. As in the previous cases, the neutrino flux is unobservably small along the rapid-annihilation funnel, but may be observable along the EWSB boundary strip for $\tan\beta = 20$. We note that a portion of the IceCube/DeepCore-friendly region for $\tan\beta = 20$ is favoured by $g_\mu - 2$. For $\tan\beta = 55$, muon fluxes are $\gtrsim 10$ /km^2/yr for $m_{1/2} \lesssim 500$ GeV along the transition/funnel and compatible with $g - 2$. We note that this case is also interesting because in much of the allowable plane capture is dominated by spin-independent scattering.

E. NUHM1 (m_A, m_0) Planes

Figure 7 shows some sample NUHM1 (m_A, m_0) planes with fixed $\tan\beta$ that exhibit rapid-annihilation funnels. In these cases, the funnels appear as essentially vertical double strips on either side of the line where $m_A = 2m_\chi$. In each case, we also note the presences of WMAP-compatible strips close to the EWSB boundary where $\mu^2 = 0$. The two are attached by coannihilation strips at $m_0 \sim 100$ GeV. When $m_{1/2} = 500$ GeV, coannihilation to the left of the funnel at low m_A is dominated by selectrons/smuons which are the LSPs in the lower left corners. In the upper left panel for $\tan\beta = 10$ and $m_{1/2} = 300$ GeV, we also see a region at low m_0 that is favoured by $g_\mu - 2$, but this is in a region disfavoured by the LEP Higgs limit. In this plane, the only WMAP-compatible region allowed by the other constraints is up the funnel at large m_0, where the neutrino flux in unobservably low. In the upper right panel for $m_{1/2} = 500$ GeV, the Higgs constraint is irrelevant, but the neutrino flux is still very low in all the WMAP-compatible region except along the strip close to the EWSB boundary. The same is true in the lower left plot for $\tan\beta = 20$ and $m_{1/2} = 500$ GeV, where we note that a part of this strip is inside the region favoured by $g_\mu - 2$. However, as shown in the lower right plot, when $\tan\beta$ is increased to 55 with the same value of $m_{1/2}$, the EWSB boundary moves so close to the rapid-annihilation funnel that there is no IceCube/DeepCore-friendly region.

F. NUHM1 Summary

We have found in the above analysis that interesting neutrino fluxes may arise from enhanced Higgsino-gaugino mixing. This possibility arose in the CMSSM in the focus-point region along the EWSB boundary, but may arise in regions of the NUHM1 parameter space that are far from this boundary, corresponding in general to larger values of $m_{1/2}$. The EWSB boundary region may also yield interesting fluxes when $\mu^2 \to 0$ at the boundary. One of the other mechanisms present in the NUHM1 for bring the relic LSP density into the WMAP-compatible range is rapid annihilation through direct-channel Higgs poles. However, we have found that this region generally yields low neutrino fluxes.

IV. REPRESENTATIVE STUDIES IN THE NUHM2

As discussed earlier, in the NUHM2 we are free to adjust both soft Higgs masses independently and as a consequence we can study models for which both μ and m_A are free parameters [43]. We first consider some (μ, m_A) planes for $A_0 = 0, m_{1/2} = 300$ GeV and $m_0 = 100$ GeV as shown in Figure 8. In each case, we see a WMAP-compatible rapid-annihilation funnel at $m_A \sim 250$ GeV as the neutralino mass is roughly 0.43 $m_{1/2}$ and

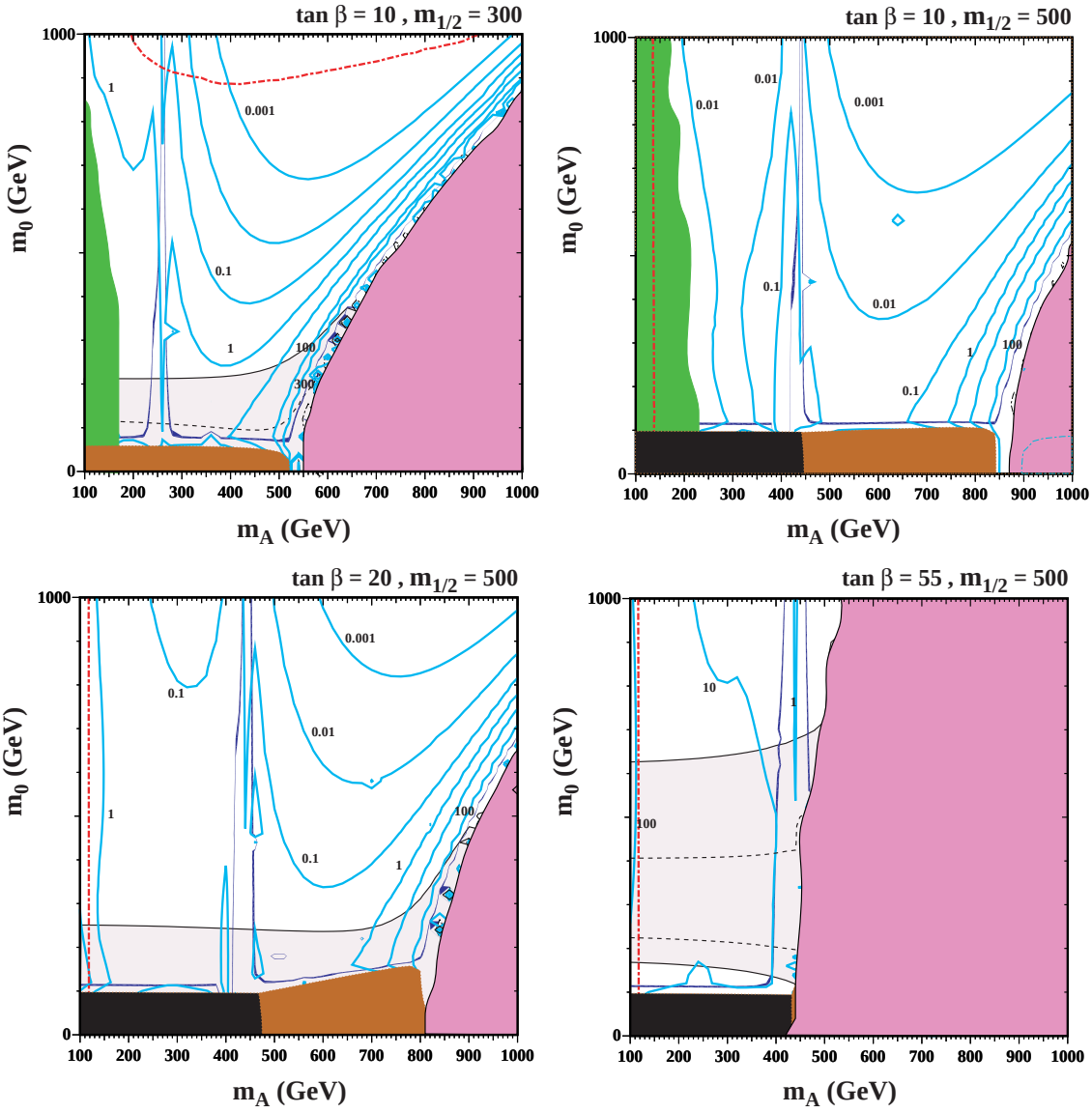

FIG. 7: *The* (m_A, m_0) *planes in the NUHM1 for* $A_0 = 0$ *and (upper row)* $\tan\beta = 10$ *and (left)* $m_{1/2} = 300$ *GeV, (right)* $m_{1/2} = 500$ *GeV, and (lower row) for* $m_{1/2} = 500$ *GeV and (left)* $\tan\beta = 20$*, (right)* $\tan\beta = 55$*. The shadings and contours have the same meanings as in Figure 5.*

therefore roughly half the pseudoscalar mass across the plane. In addition there is an arc at relatively large μ and m_A due to the coannihilations between the neutralino and sneutrinos. The dark blue shaded regions have a sneutrino LSP and are excluded [44]. In the left panel for $\tan\beta = 10$, we also see a near-vertical strip at low μ where the LSP has a substantial Higgsino component, which extends downwards in a stau coannihilation strip almost parallel to the charged dark LSP boundary. The $\mu > 0$ half of the plane is consistent with the $g-2$ constraint. As we have seen before, equilibrium is in this case well established along the vertical transition strip, partially established along the horizontal funnel, and not at all along the arcing coannihilation strip. While scattering is heavily dominated by the spin-dependent cross-section along the transition strip, spin-independent scattering is significant along the

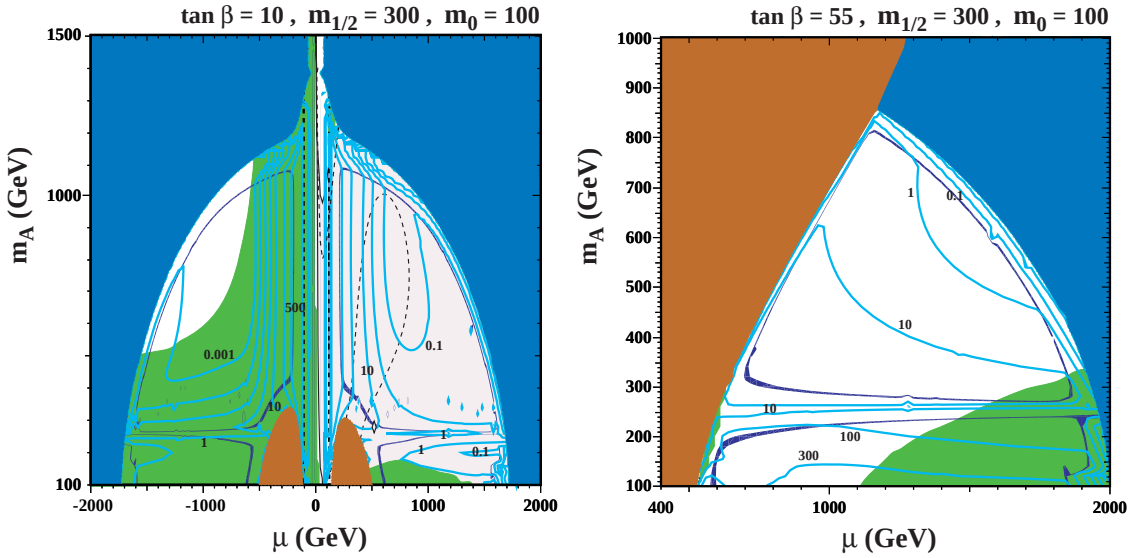

FIG. 8: *The* (μ, m_A) *planes in the NUHM2 for* $A_0 = 0, m_{1/2} = 300$ *GeV and* $m_0 = 100$ *GeV with (left)* $\tan\beta = 10$ *and (right)* $\tan\beta = 55$. *In the blue shaded regions the LSP is a sneutrino, and the other shadings and contours have the same meanings as in Figure 3.*

other two strips. In the right panel for $\tan\beta = 55$, the charged LSP boundary is present at lower μ and more prevalent at large m_A. Both the stau and sneutino LSP regions are again parallelled by WMAP-compatible coannihilation strips. The supersymmetric contribution to $g-2$ in the right panel exceeds the 2σ bound.

In the left plane, the only region with an IceCube/DeepCore-friendly neutrino flux is the vertical strip with a substantial Higgsino content, analogous to those seen previously in our NUHM1 analysis. Here fluxes are in excess of 500 /km^2/yr. On the other hand, in the right panel where this strip has disappeared, the only IceCube/DeepCore-friendly region is at small μ and m_A, below the rapid-annihilation funnel. We further note that, in both planes, the Higgs mass falls below 114 GeV.

Similar trends can be seen in Figure 9 for $A_0 = 0, m_{1/2} = 500$ GeV and $m_0 = 300$ GeV. In the left panel for $\tan\beta = 10$, we see a near-vertical strip where the LSP has an enhanced Higgsino component, split in two by a near-horizontal rapid-annihilation funnel. This funnel is also present in the right panel for $\tan\beta = 55$, and splits a diagonal coannihilation strip close to the charged LSP boundary. Again, as in the previous case for smaller $m_{1/2}$ and m_0, the only IceCube/DeepCore-friendly regions are in the Higgsino-like strip at small μ for $\tan\beta = 10$, and for very small μ and m_A for $\tan\beta = 55$. Spin-independent scattering becomes dominant for $|\mu| \gtrsim 500$ GeV when $\tan\beta = 10$ and is dominant everywhere in the displayed plane for $\tan\beta = 55$. In this case, the Higgs mass is above 114 GeV everywhere above the red dot dashed curved found at low m_A. For $\tan\beta = 10$, the supersymmetric contribution to $g-2$ is too small across the plane, whereas for $\tan\beta = 55$ it lies within the experimental range.

Finally, we present some (m_1, m_2) planes in Figs. 10 and 11, for $m_{1/2} = 300$ GeV, $m_0 = 100$ GeV and $m_{1/2} = 500$ GeV, $m_0 = 300$ GeV, respectively. In each case, we assume $A_0 = 0$ and the left panel is for $\tan\beta = 10$ and the right panel for $\tan\beta = 55$. The ranges of m_1 and m_2 are symmetric $\in (-1000, 1000)$ GeV, except for the right panel of Figure 10, where asymmetric ranges $(m_1, m_2) \in (-2000, 0)$ GeV are chosen so as to display better the regions

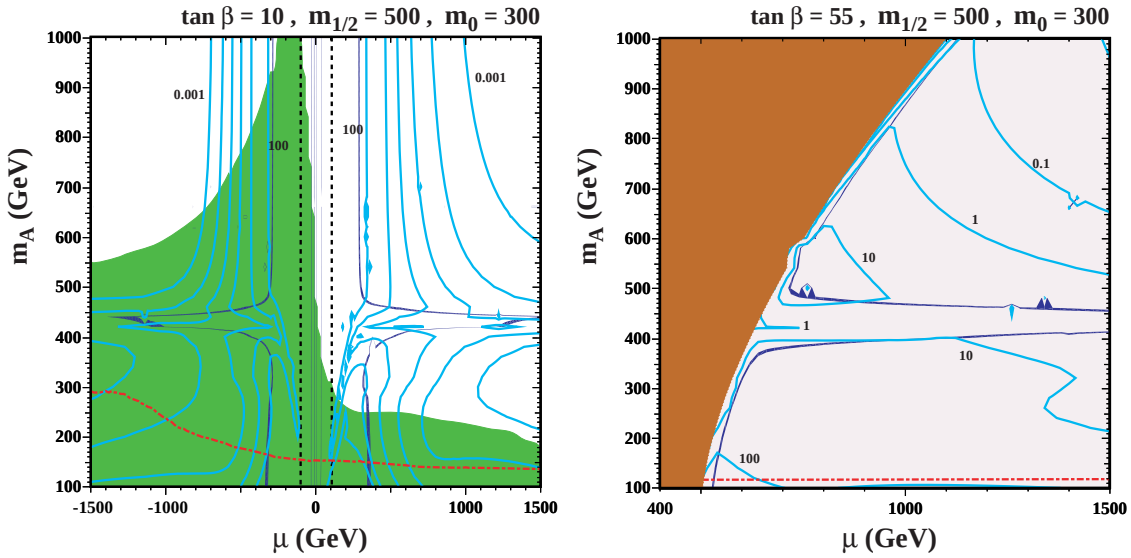

FIG. 9: *The* (μ, m_0) *planes in the NUHM2 for* $A_0 = 0, m_{1/2} = 500$ *GeV and* $m_0 = 300$ *GeV with (left)* $\tan\beta = 10$ *and (right)* $\tan\beta = 55$. *The shadings and contours have the same meanings as in Figure 3.*

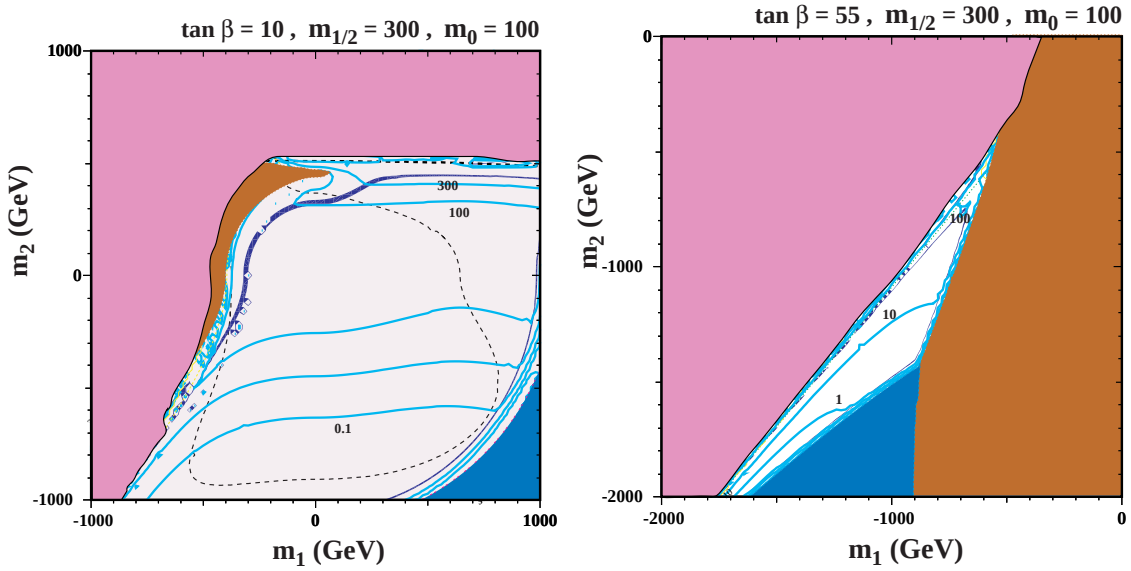

FIG. 10: *The* (m_1, m_2) *planes in the NUHM2 for* $m_{1/2} = 300$ *GeV and* $m_0 = 100$ *GeV with (left)* $\tan\beta = 10$ *and (right)* $\tan\beta = 55$. *The signs shown for* m_i *actually refer to the sign of* m_i^2 *as they are run in the RGEs. The shadings and contours have the same meanings as in Figure 8.*

not excluded by the EWSB constraint (pink) and the sneutrino LSP regions (blue) or the charged-LSP constraint (brown). The signs shown for m_i actually refer to the sign of m_i^2 as they are run in the RGEs. As these are GUT scale parameters, negative values may indicate a cosmological issue with broken symmetric vacua. For a recent discussion of this issue in the NUHM, see [45].

In the left panel of Figure 10 for $\tan\beta = 10$, we see two narrow WMAP strips following

the top left and bottom right boundaries of the allowed lozenge of the (m_1, m_2) plane. Of these, the former has an IceCube/DeepCore-friendly neutrino-induced muon flux over most of its length, rising to > 300 events/km^2/yr for $m_2 \sim 400$ GeV. Note that the nearly horizontal part of the strip corresponds again to the transition strip where a there significant Higgsino contribution to the neutralino composition. The more vertical part of the strip corresponds to the rapid annihilation funnel. On the other hand, the bottom right WMAP strip corresponding to neutralino-sneutrino coannihilation generally has an unobservably small neutrino flux, except for positive values of m_2, where the muon flux may reach 30 events/km^2/yr. As usual, the larger neutrino fluxes are reached when the Higgsino component of the LSP is enhanced. In this plane the $g-2$ constraint is satisfied, though the Higgs mass is low.

In the right panel of Figure 10 for $\tan\beta = 55$, the allowed region of the (m_1, m_2) plane has receded to more negative values of m_1 and m_2, and the two narrow WMAP strips are squeezed closer together. Additionally, we note that the top left strip has bifurcated along the two sides of a rapid-annihilation funnel, whereas the lower right strip follows either the stau or sneutrino coannihilation boundaries. As in the left panel of Figure 10, the neutrino fluxes are generally more favourable along the top left strip, though they also become more IceCube/DeepCore-friendly towards the upper end of the other strip, near their junction. Neither $g-2$ or the Higgs mass constraints are satisfied in this plane.

In the left panel of Figure 11 for $\tan\beta = 10$, we see a single narrow WMAP strip following the top boundary of the allowed region of the (m_1, m_2) plane corresponding to the transition strip. As in the corresponding panel of Figure 10, the neutrino-induced muon flux is largest, exceeding 100 events/km^2/yr and hence quite IceCube/DeepCore-friendly, in the top part of the strip close to the EWSB boundary where $m_2 \sim 800$ GeV and the LSP has an enhanced Higgsino component. The left boundary corresponds to the the funnel region where there are two strips, one of which continues on to the vertical transitions strip. The upper part of the funnel still has observable fluxes, but these quickly drop as m_2 is decreased. Here, and in the right panel as well, equilibrium is established along all WMAP strips, however spin-dependent scattering is sub-dominant almost everywhere in the plane.

In the right panel of Figure 11 for $\tan\beta = 55$, the previous single narrow WMAP strip has again bifurcated along the two sides of a rapid-annihilation funnel, and has moved away from the boundaries of the allowed region of the (m_1, m_2) plane. Once again, the neutrino flux is largest for $m_2 > 0$, though generally lower than in the left panel of Figure 11 (where $\tan\beta$ is smaller) or in the right panel of Figure 10 (where $m_{1/2}$ and m_0 are smaller), and only barely IceCube/DeepCore-friendly. In this plane, both the $g-2$ and Higgs mass constraints are satisfied.

V. SUMMARY

In our previous analysis of the CMSSM, we found that the flux of high-energy neutrinos from LSP annihilations inside the Sun was likely to be observable along the focus-point WMAP strip, where the Higgsino component of the LSP is enhanced, and at the tip of the coannihilation WMAP strip where the LSP is relatively light. On the other hand, there were significant portions of the WMAP-compatible strips in parameter space, particularly along the coannihilation strip and heavy-Higgs rapid-annihilation funnels, where the the neutrino flux was not IceCube/DeepCore-friendly.

We find some similar features in our analyses of the NUHM1 and NUHM2. Specifically,

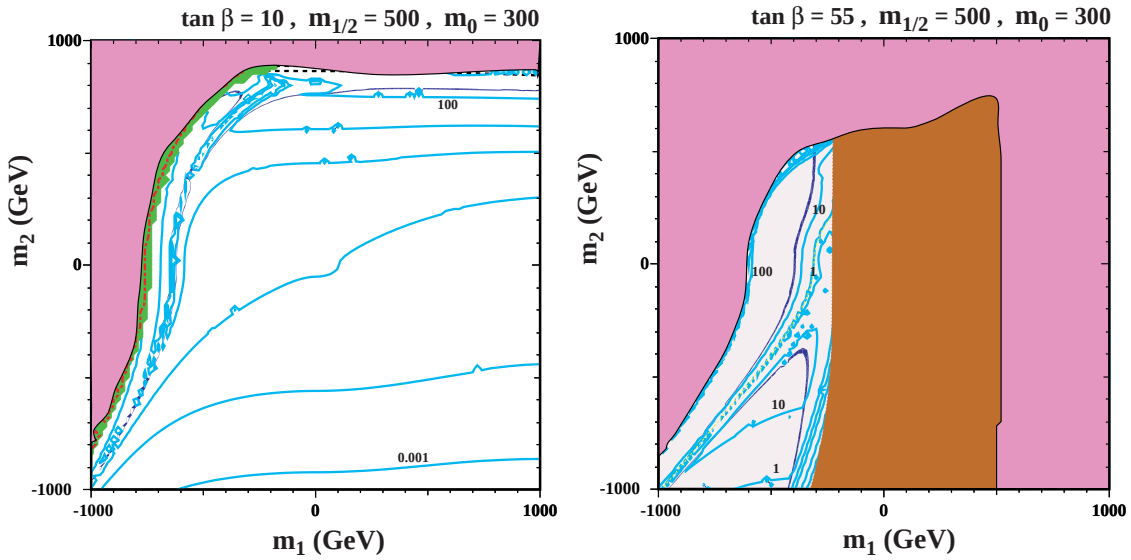

FIG. 11: *The* (m_1, m_2) *planes in the NUHM2 for* $m_{1/2} = 500$ *GeV and* $m_0 = 300$ *GeV with (left)* $\tan\beta = 10$ *and (right)* $\tan\beta = 55$. *The shadings and contours have the same meanings as in Figure 3.*

there are significant portions of the WMAP strips where the high-energy solar neutrino flux is unlikely to be observable with IceCube/DeepCore. In these models, IceCube/DeepCore-friendly fluxes are often found in regions where the LSP has an enhanced Higgsino component, and this occurs under circumstances that cannot be realized in the CMSSM. Specifically, it may occur for larger LSP masses than along the focus-point strip of the CMSSM: see, for example, the right panel of Figure 3, the first three panels of Figure 4, and the first three panels of Figure 5.

We conclude, therefore, that IceCube/DeepCore has interesting prospects for probing aspects of the NUHM1 and NUHM2 parameter spaces. However, it seems clear that a more complete exploration of these models, capable of measuring a high-energy neutrino flux when the LSP is relatively heavy and/or does not have a large Higgsino component, would require a subsequent generation of experiment. On the other hand, one may hope that forthcoming LHC results and/or direct searches for LSP scattering could provide more encouraging indications on the prospects for searches for supersymmetric dark matter via annihilation into high-energy solar neutrinos.

Acknowledgments

The work of KAO was supported in part by DOE Grant No. DE-FG02-94ER-40823. KAO also thanks SLAC (supported by the DOE under contract number DE-AC02-76SF00515) and the Stanford Institute for Theoretical Physics for their hospitality and support while this work was being finished. C.S. is grateful for financial support from the Swedish Research Council (VR) through the Oskar Klein Centre and thanks the William I. Fine Theoretical Physics Institute at the University of Minnesota, where part of this work was performed, for its hospitality. C.S. also thanks M. Danninger for useful discussions regarding IceCube/DeepCore. The work of V.C.S. was supported by Marie Curie International Rein-

tegration grant SUSYDM-PHEN, MIRG-CT-2007-203189.

---

[1] J. Silk, K. A. Olive and M. Srednicki, Phys. Rev. Lett. **55**, 257 (1985); M. Srednicki, K. A. Olive and J. Silk, Nucl. Phys. B **279**, 804 (1987); J. S. Hagelin, K. W. Ng and K. A. Olive, Phys. Lett. B **180**, 375 (1986); K. W. Ng, K. A. Olive and M. Srednicki, Phys. Lett. B **188**, 138 (1987); T. K. Gaisser, G. Steigman and S. Tilav, Phys. Rev. D **34**, 2206 (1986); F. Halzen, T. Stelzer and M. Kamionkowski, Phys. Rev. D **45**, 4439 (1992); L. Bergstrom, J. Edsjo and P. Gondolo, Phys. Rev. D **55**, 1765 (1997) [arXiv:hep-ph/9607237]; K. Freese and M. Kamionkowski, Phys. Rev. D **55**, 1771 (1997) [arXiv:hep-ph/9609370].

[2] K. Freese, Phys. Lett. B **167**, 295 (1986); L. M. Krauss, M. Srednicki and F. Wilczek, Phys. Rev. D **33**, 2079 (1986).

[3] J. Ahrens *et al.* [IceCube Collaboration], Astropart. Phys. **20**, 507 (2004) [arXiv:astro-ph/0305196].

[4] A. Achterberg *et al.* [IceCube Collaboration], Astropart. Phys. **26**, 155 (2006) [arXiv:astro-ph/0604450].

[5] E. Resconi, for the IceCube Collaboration, Nucl. Instrum. Meth. A **602**, 7 (2009) [arXiv:0807.3891 [astro-ph]].

[6] R. Abbasi *et al.* [IceCube Collaboration], Phys. Rev. Lett. **102**, 201302 (2009) [arXiv:0902.2460v2 [astro-ph.CO]]; the combined IceCube/DeepCore flux sensitivities are found in Figure 3 of the arXiv version 2.

[7] J. Ellis, K. A. Olive, C. Savage and V. C. Spanos, Phys. Rev. D **81**, 085004 (2010) [arXiv:0912.3137 [hep-ph]].

[8] M. Drees and M. M. Nojiri, Phys. Rev. D **47**, 376 (1993) [arXiv:hep-ph/9207234]; H. Baer and M. Brhlik, Phys. Rev. D **53**, 597 (1996) [arXiv:hep-ph/9508321]; H. Baer and M. Brhlik, Phys. Rev. D **57**, 567 (1998) [arXiv:hep-ph/9706509]; J. R. Ellis, T. Falk, K. A. Olive and M. Schmitt, Phys. Lett. B **388**, 97 (1996) [arXiv:hep-ph/9607292]; J. R. Ellis, T. Falk, K. A. Olive and M. Schmitt, Phys. Lett. B **413**, 355 (1997) [arXiv:hep-ph/9705444]; J. R. Ellis, T. Falk, G. Ganis, K. A. Olive and M. Schmitt, Phys. Rev. D **58**, 095002 (1998) [arXiv:hep-ph/9801445]; V. D. Barger and C. Kao, Phys. Rev. D **57**, 3131 (1998) [arXiv:hep-ph/9704403]; J. R. Ellis, T. Falk, G. Ganis and K. A. Olive, Phys. Rev. D **62**, 075010 (2000) [arXiv:hep-ph/0004169]; J. R. Ellis, T. Falk, G. Ganis, K. A. Olive and M. Srednicki, Phys. Lett. B **510**, 236 (2001) [arXiv:hep-ph/0102098]; V. D. Barger and C. Kao, Phys. Lett. B **518**, 117 (2001) [arXiv:hep-ph/0106189]; L. Roszkowski, R. Ruiz de Austri and T. Nihei, JHEP **0108**, 024 (2001) [arXiv:hep-ph/0106334]; A. B. Lahanas and V. C. Spanos, Eur. Phys. J. C **23**, 185 (2002) [arXiv:hep-ph/0106345]; A. Djouadi, M. Drees and J. L. Kneur, JHEP **0108**, 055 (2001) [arXiv:hep-ph/0107316]; U. Chattopadhyay, A. Corsetti and P. Nath, Phys. Rev. D **66**, 035003 (2002) [arXiv:hep-ph/0201001]; J. R. Ellis, K. A. Olive and Y. Santoso, New J. Phys. **4**, 32 (2002) [arXiv:hep-ph/0202110]; H. Baer, C. Balazs, A. Belyaev, J. K. Mizukoshi, X. Tata and Y. Wang, JHEP **0207**, 050 (2002) [arXiv:hep-ph/0205325]; R. Arnowitt and B. Dutta, arXiv:hep-ph/0211417.

[9] E. Komatsu *et al.* [WMAP Collaboration], Astrophys. J. Suppl. **192** (2011) 18 [arXiv:1001.4538 [astro-ph.CO]].

[10] J. R. Ellis, K. A. Olive, Y. Santoso and V. C. Spanos, Phys. Lett. B **565**, 176 (2003) [arXiv:hep-ph/0303043];

[11] H. Baer and C. Balazs, JCAP **0305**, 006 (2003) [arXiv:hep-ph/0303114]; A. B. Lahanas and D. V. Nanopoulos, Phys. Lett. B **568**, 55 (2003) [arXiv:hep-ph/0303130]; U. Chattopadhyay, A. Corsetti and P. Nath, Phys. Rev. D **68**, 035005 (2003) [arXiv:hep-ph/0303201]; C. Munoz, Int. J. Mod. Phys. A **19**, 3093 (2004) [arXiv:hep-ph/0309346]; R. L. Arnowitt, B. Dutta and B. Hu, arXiv:hep-ph/0310103.

[12] A. Corsetti and P. Nath, Int. J. Mod. Phys. A **15**, 905 (2000) [arXiv:hep-ph/9904497]; J. L. Feng, K. T. Matchev and F. Wilczek, Phys. Rev. D **63**, 045024 (2001) [arXiv:astro-ph/0008115]; V. D. Barger, F. Halzen, D. Hooper and C. Kao, Phys. Rev. D **65**, 075022 (2002) [arXiv:hep-ph/0105182]; H. Baer, A. Belyaev, T. Krupovnickas and J. O'Farrill, JCAP **0408**, 005 (2004) [arXiv:hep-ph/0405210]; R. Trotta, R. R. de Austri and C. P. d. Heros, JCAP **0908**, 034 (2009) [arXiv:0906.0366 [astro-ph.HE]].

[13] H. Baer, A. Mustafayev, S. Profumo, A. Belyaev and X. Tata, Phys. Rev. D **71**, 095008 (2005) [arXiv:hep-ph/0412059]; H. Baer, A. Mustafayev, S. Profumo, A. Belyaev and X. Tata, JHEP **0507**, 065 (2005) [arXiv:hep-ph/0504001].

[14] J. R. Ellis, K. A. Olive and P. Sandick, Phys. Rev. D **78**, 075012 (2008) [arXiv:0805.2343 [hep-ph]].

[15] D. Matalliotakis and H. P. Nilles, Nucl. Phys. B **435**, 115 (1995) [arXiv:hep-ph/9407251]; M. Olechowski and S. Pokorski, Phys. Lett. B **344**, 201 (1995) [arXiv:hep-ph/9407404]; V. Berezinsky, A. Bottino, J. R. Ellis, N. Fornengo, G. Mignola and S. Scopel, Astropart. Phys. **5**, 1 (1996) [arXiv:hep-ph/9508249]; M. Drees, M. M. Nojiri, D. P. Roy and Y. Yamada, Phys. Rev. D **56**, 276 (1997) [Erratum-ibid. D **64**, 039901 (2001)] [arXiv:hep-ph/9701219]; M. Drees, Y. G. Kim, M. M. Nojiri, D. Toya, K. Hasuko and T. Kobayashi, Phys. Rev. D **63**, 035008 (2001) [arXiv:hep-ph/0007202]; P. Nath and R. L. Arnowitt, Phys. Rev. D **56**, 2820 (1997) [arXiv:hep-ph/9701301]; J. R. Ellis, T. Falk, G. Ganis, K. A. Olive and M. Schmitt, Phys. Rev. D **58**, 095002 (1998) [arXiv:hep-ph/9801445]; J. R. Ellis, T. Falk, G. Ganis and K. A. Olive, Phys. Rev. D **62**, 075010 (2000) [arXiv:hep-ph/0004169]; A. Bottino, F. Donato, N. Fornengo and S. Scopel, Phys. Rev. D **63**, 125003 (2001) [arXiv:hep-ph/0010203]; S. Profumo, Phys. Rev. D **68**, 015006 (2003) [arXiv:hep-ph/0304071]; D. G. Cerdeno and C. Munoz, JHEP **0410**, 015 (2004) [arXiv:hep-ph/0405057].

[16] J. R. Ellis, K. A. Olive and Y. Santoso, Phys. Lett. B **539**, 107 (2002) [arXiv:hep-ph/0204192]; J. R. Ellis, T. Falk, K. A. Olive and Y. Santoso, Nucl. Phys. B **652**, 259 (2003) [arXiv:hep-ph/0210205].

[17] Z. Ahmed *et al.* [The CDMS-II Collaboration], Science **327**, 1619 (2010) [arXiv:0912.3592 [astro-ph.CO]].

[18] E. Aprile *et al.* [XENON100 Collaboration], Phys. Rev. Lett. **105**, 131302 (2010) [arXiv:1005.0380 [astro-ph.CO]].

[19] V. Khachatryan *et al.* [CMS Collaboration], Phys. Lett. B **698**, 196 (2011) [arXiv:1101.1628 [hep-ex]].

[20] G. Aad *et al.* [ATLAS Collaboration], in preparation; see `https://twiki.cern.ch/twiki/bin/view/AtlasPublic/SusyPublicResults`.

[21] O. Buchmueller *et al.*, JHEP **0809**, 117 (2008) [arXiv:0808.4128 [hep-ph]]; O. Buchmueller *et al.*, Eur. Phys. J. C **64**, 391 (2009) [arXiv:0907.5568 [hep-ph]].

[22] O. Buchmueller *et al.*, Eur. Phys. J. C **71**, 1583 (2011) [arXiv:1011.6118 [hep-ph]].

[23] S. Chen *et al.* [CLEO Collaboration], Phys. Rev. Lett. **87**, 251807 (2001) [arXiv:hep-ex/0108032]; P. Koppenburg *et al.* [Belle Collaboration], Phys. Rev. Lett. **93**, 061803 (2004) [arXiv:hep-ex/0403004]; B. Aubert *et al.* [BaBar Collaboration],

arXiv:hep-ex/0207076; E. Barberio *et al.* [Heavy Flavor Averaging Group (HFAG)], arXiv:hep-ex/0603003.

[24] Joint LEP 2 Supersymmetry Working Group, *Combined LEP Chargino Results up to 208 GeV*, `http://lepsusy.web.cern.ch/lepsusy/www/inos_moriond01/charginos_pub.html`.

[25] R. Barate *et al.* [ALEPH, DELPHI, L3, OPAL Collaborations: the LEP Working Group for Higgs boson searches], Phys. Lett. B **565**, 61 (2003) [arXiv:hep-ex/0306033]; D. Zer-Zion, *Prepared for 32nd International Conference on High-Energy Physics (ICHEP 04), Beijing, China, 16-22 Aug 2004*, World Scientific, Hackensack (2005); ALEPH, DELPHI, L3, OPAL Collaborations: the LEP Working Group for Higgs boson searches, LHWG-NOTE-2004-01, ALEPH-2004-008, DELPHI-2004-042, L3-NOTE-2820, OPAL-TN-744, `http://lephiggs.web.cern.ch/LEPHIGGS/papers/August2004_MSSM/index.html`.

[26] S. Heinemeyer, W. Hollik and G. Weiglein, Comput. Phys. Commun. **124**, 76 (2000) [arXiv:hep-ph/9812320]; S. Heinemeyer, W. Hollik and G. Weiglein, Eur. Phys. J. C **9**, 343 (1999) [arXiv:hep-ph/9812472]; G. Degrassi, S. Heinemeyer, W. Hollik, P. Slavich and G. Weiglein, Eur. Phys. J. C **28**, 133 (2003) [arXiv:hep-ph/0212020]; M. Frank, T. Hahn, S. Heinemeyer, W. Hollik, H. Rzehak and G. Weiglein, JHEP **0702**, 047 (2007) [arXiv:hep-ph/0611326]; `http://www.feynhiggs.de/`

[27] G. W. Bennett *et al.* [Muon G-2 Collaboration], Phys. Rev. D **73**, 072003 (2006) [arXiv:hep-ex/0602035].

[28] B. Aubert *et al.* [BABAR Collaboration], Phys. Rev. Lett. **103**, 231801 (2009) [arXiv:0908.3589 [hep-ex]].

[29] M. Davier, A. Hoecker, B. Malaescu and Z. Zhang, Eur. Phys. J. C **71**, 1515 (2011) [arXiv:1010.4180 [hep-ph]].

[30] A. Bottino, F. Donato, N. Fornengo and S. Scopel, Astropart. Phys. **13**, 215 (2000) [arXiv:hep-ph/9909228].

[31] E. Accomando, R. L. Arnowitt, B. Dutta and Y. Santoso, Nucl. Phys. B **585**, 124 (2000) [arXiv:hep-ph/0001019].

[32] J. R. Ellis, K. A. Olive, Y. Santoso and V. C. Spanos, Phys. Rev. D **71**, 095007 (2005) [arXiv:hep-ph/0502001].

[33] J. R. Ellis, K. A. Olive and C. Savage, Phys. Rev. D **77**, 065026 (2008) [arXiv:0801.3656 [hep-ph]].

[34] V. Niro, A. Bottino, N. Fornengo and S. Scopel, Phys. Rev. D **80**, 095019 (2009) [arXiv:0909.2348 [hep-ph]].

[35] M. Alekseev *et al.* [COMPASS Collaboration], Phys. Lett. B **660**, 458 (2008) [arXiv:0707.4077 [hep-ex]].

[36] A. Serenelli, S. Basu, J. W. Ferguson and M. Asplund, Astrophys. J. **705**, L123 (2009) [arXiv:0909.2668 [astro-ph.SR]].

[37] M. Asplund, N. Grevesse, A. J. Sauval and P. Scott, Ann. Rev. Astron. Astrophys. **47**, 481 (2009) [arXiv:0909.0948 [astro-ph.SR]].

[38] A. Gould, Astrophys. J. **388**, 338 (1992).

[39] V. Barger, Y. Gao and D. Marfatia, Phys. Rev. D **83**, 055012 (2011) [arXiv:1101.4410 [hep-ph]].

[40] M. Danninger, private correspondence.

[41] M. Blennow, J. Edsjo and T. Ohlsson, JCAP **0801**, 021 (2008) [arXiv:0709.3898 [hep-ph]]; J. Edsjo, WimpSim Neutrino Monte Carlo, `http://www.physto.se/~edsjo/wimpsim/`

[42] P. Gondolo, J. Edsjo, P. Ullio, L. Bergstrom, M. Schelke and E. A. Baltz, JCAP **0407**, 008

(2004) [arXiv:astro-ph/0406204]; P. Gondolo, J. Edsjo, P. Ullio, L. Bergstrom, M. Schelke, E. A. Baltz, T. Bringmann and G. Duda, `http://www.physto.se/~edsjo/darksusy/`

[43] For a recent study within the NUHM2, see: M. A. Ajaib, I. Gogoladze and Q. Shafi, arXiv:1101.0835 [hep-ph].

[44] T. Falk, K. A. Olive and M. Srednicki, Phys. Lett. B **339**, 248 (1994) [arXiv:hep-ph/9409270]; C. Arina and N. Fornengo, JHEP **0711**, 029 (2007) [arXiv:0709.4477 [hep-ph]].

[45] J. R. Ellis, J. Giedt, O. Lebedev, K. Olive and M. Srednicki, Phys. Rev. D **78**, 075006 (2008) [arXiv:0806.3648 [hep-ph]].